

# Regulated Polarization Degree of Upconversion Luminescence and Multiple Anti-Counterfeit Applications

*Dongping Wen<sup>a</sup>, Yi Liang<sup>a</sup>, Xiaoming Mo<sup>a</sup>, Caofeng Pan<sup>a,b\*</sup> and Ping Chen<sup>a\*</sup>*

<sup>a</sup> Center on Nanoenergy Research, Guangxi Key Laboratory for Relativistic Astrophysics, School of Physical Science and Technology, Guangxi University, Nanning 530004, P. R. China

<sup>b</sup> CAS Center for Excellence in Nanoscience, Beijing Key Laboratory of Micronano Energy and Sensor, Beijing Institute of Nanoenergy and Nanosystems, Chinese Academy of Sciences, Beijing, 100140, P. R. China

**Email:** chenping@gxu.edu.cn; cfpan@binn.cas.cn

## Keywords

polarized upconversion luminescence, degree of polarization, the population density of excited state, the number of upconversion photons, polarization anti-counterfeiting display

## Abstract

Polarized upconversion luminescence (PUCL) of lanthanide ( $\text{Ln}^{3+}$ ) ions has been widely used in single particle tracking, microfluidics detection, three-dimensional displays, and so on. However, no effective strategy has been developed for modulating PUCL. Here, we report a strategy to regulate PUCL in  $\text{Ho}^{3+}$ -doped  $\text{NaYF}_4$  single nanorods based on the number of upconversion photons. By constructing a multiphoton upconversion system for  $\text{Ho}^{3+}$ , we regulate the degree of polarization (DOP) of PUCL from 0.6 for two-photon luminescence to 0.929 for three-photon upconversion luminescence (UCL). Furthermore, our strategy is verified by cross-relaxation between  $\text{Ho}^{3+}$  and  $\text{Yb}^{3+}$ , excitation wavelength, excitation power density, and local site symmetry. And this regulation strategy of PUCL has also been achieved in  $\text{Tm}^{3+}$ , where DOP is ranged from 0.233 for two-photon luminescence to 0.925 for four-photon UCL. Besides, multi-dimensional anti-counterfeiting display has been explored with PUCL. This work provides an effective strategy for the regulation of PUCL and also provides more opportunities for the development of polarization display, optical encoding, anti-counterfeiting, and integrated optical devices.

## 1. Introduction

Polarized upconversion luminescence (PUCL) of lanthanide ions ( $\text{Ln}^{3+}$ ) is the anisotropic emission induced by the local site symmetry around  $\text{Ln}^{3+}$ .<sup>[1-3]</sup> PUCL has developed applications in optical storage, biological imaging, polarization displays, and biotracking.<sup>[4-9]</sup> The adjustable polarized luminescence from  $\text{Ln}^{3+}$  can provide a strong guarantee for biological probes and three-dimensional display.<sup>[10-14]</sup> In particular, highly PUCL has great potential in multiple anti-counterfeiting encryption and display.<sup>[15-21]</sup> However, due to the diversity of  $\text{Ln}^{3+}$  ions and the complexity of the electronic structure of

trivalent  $4f$  ions,<sup>[22]</sup> there is no effective control strategy for controlling the PUCL. The polarized luminescence of  $\text{Ln}^{3+}$  is influenced not only by the local site symmetry of the crystal field (CF) but also by many other factors, such as the direction of the electric field of the excitation field, the energy transfer between  $\text{Ln}^{3+}$ , the concentration of activators, plasmonic nanomaterials with a specific structure, and so on.<sup>[23-28]</sup> In order to control the polarized luminescence of  $\text{Ln}^{3+}$  from a single nanorod, attempts have been made to vary the concentration of sensitizers and activators.<sup>[23,24]</sup> However, it is still difficult to tune PUCL and achieve highly polarized luminescence from  $\text{Ln}^{3+}$ .

Site symmetry is around  $\text{Ln}^{3+}$ , which is essential for PUCL.<sup>[1-3]</sup> In the hexagonal phase of  $\text{NaYF}_4$ , point group symmetry is  $C_6$ , and the energy states of  $\text{Ln}^{3+}$  are represented by the different irreducible  $\Gamma_n$ .<sup>[29]</sup> Electrons are pumped from the ground state (GS) to the excited state (ES)  $^{2s+1}L_J$ , which is split into different Stark energy levels and presented as irreducible ( $\Gamma_n$ ). The ES undergoes a non-radiative (NR) or radiative transition and decays to the GS. This essential process for radiative transition is an irreducible transition from  $\Gamma_n$  (ES)  $\rightarrow$   $\Gamma_m$  (GS) ( $m \neq n$ ).<sup>[30]</sup> Some transition dipoles, such as  $\sigma$  and  $\pi$  configurations, exhibit excitation polarization dependence or emission anisotropy.<sup>[3,31]</sup> The polarization of the upconversion luminescence (UCL) originates from the mixture of different dipole transitions  $\Gamma_n$  (ES)  $\rightarrow$   $\Gamma_m$  (GS). Therefore, constructing an energy system for multiphoton upconversion can broaden the distribution of irreducible transitions  $\Gamma_n \rightarrow \Gamma_m$  with various mixture states at multiple ESs. Here, we choose  $\text{Ho}^{3+}$  and  $\text{Tm}^{3+}$  as activators because  $\text{Ho}^{3+}$  and  $\text{Tm}^{3+}$  possess rich ladder-type energy levels and multi-color emissions, which correspond to multiple photon upconversion processes.<sup>[32]</sup> These bring more possibilities for our regulation of excitation polarization luminescence and extending the application to multiple anti-counterfeiting displays. Despite the promising performance of  $\text{Ho}^{3+}$  and  $\text{Tm}^{3+}$ , the regulation of PUCL by the NR transitions therein remains a challenge.

In this work, we report a strategy to modulate the PUCL based on multiphoton upconversion processes. The polarization of multiple emissions is regulated by the number of photons in the multiphoton upconversion process constructed in  $\text{Ho}^{3+}$  ions, where the degree of polarization (DOP) of three-photon process is larger than that of two-photon process. With the exclusion of the CF, our mechanistic studies show that the multiphoton upconversion process can be pumped to a higher ES, which is less affected by NR transitions. The population density of higher ESs is lower, and the mixture of electron configurations for irreducible transitions  $\Gamma_n$  (ES)  $\rightarrow$   $\Gamma_m$  (GS) is fewer. That is, dipole orientations for irreducible transitions in higher ESs are not too complicated. Thus, the proportion of dipole transitions in a similar direction is larger, resulting in a larger DOP of PUCL. The DOP exhibits an inverse relationship with the population density of ESs, which determines the strength of mixed irreducible transitions  $\Gamma_n$  (ES)  $\rightarrow$   $\Gamma_m$  (GS) and mixed dipole orientations. Therefore, we can tune the DOP of PUCL by controlling the number of photons in the upconversion process. This regulatory strategy has not only been verified in  $\text{Ho}^{3+}$  but also in  $\text{Tm}^{3+}$ . The DOP is regulated from 0.925 for the four-photon process to 0.233 for the two-photon process in  $\text{NaYF}_4:\text{Tm}, \text{Yb}$  single nanorods. This highly polarized and tunable UCL is applied in multi-dimensional anti-counterfeiting displays.

## 2. Results and Discussion

### 2.1. Constructed multiphoton upconversion energy system for regulating PUCL.

In this work, we need to construct an energy system for multiphoton upconversion transitions to generate PUCL and realize polarization regulation. In the traditional multiphoton upconversion process by excited state absorption (ESA), ground state absorption (GSA) occurs once the energy resonance of the pump photon with the energy from the GS to the first ES<sub>1</sub> of  $\text{Ln}^{3+}$ . As a result, the metastable state ES<sub>1</sub> is pumped, followed by the absorption of another pumped photon by ESA to generate ES<sub>2</sub>. Then, ES<sub>2</sub> undergoes a radiative transition, producing the two-photon UCL Em<sub>1</sub> (Figure 1).<sup>[33]</sup> Analogously, ES<sub>3</sub> gives three-photon UCL, Em<sub>2</sub> and so on. According to

$$N_2 \propto N_1^2 \text{ (i.e., } N_I < 1) \quad (1),$$

where  $N_I$  and  $N_2$  are the population density of the ES<sub>1</sub> and ES<sub>2</sub>, respectively.<sup>[34]</sup> More energy state  $|i\rangle$  analogies. The

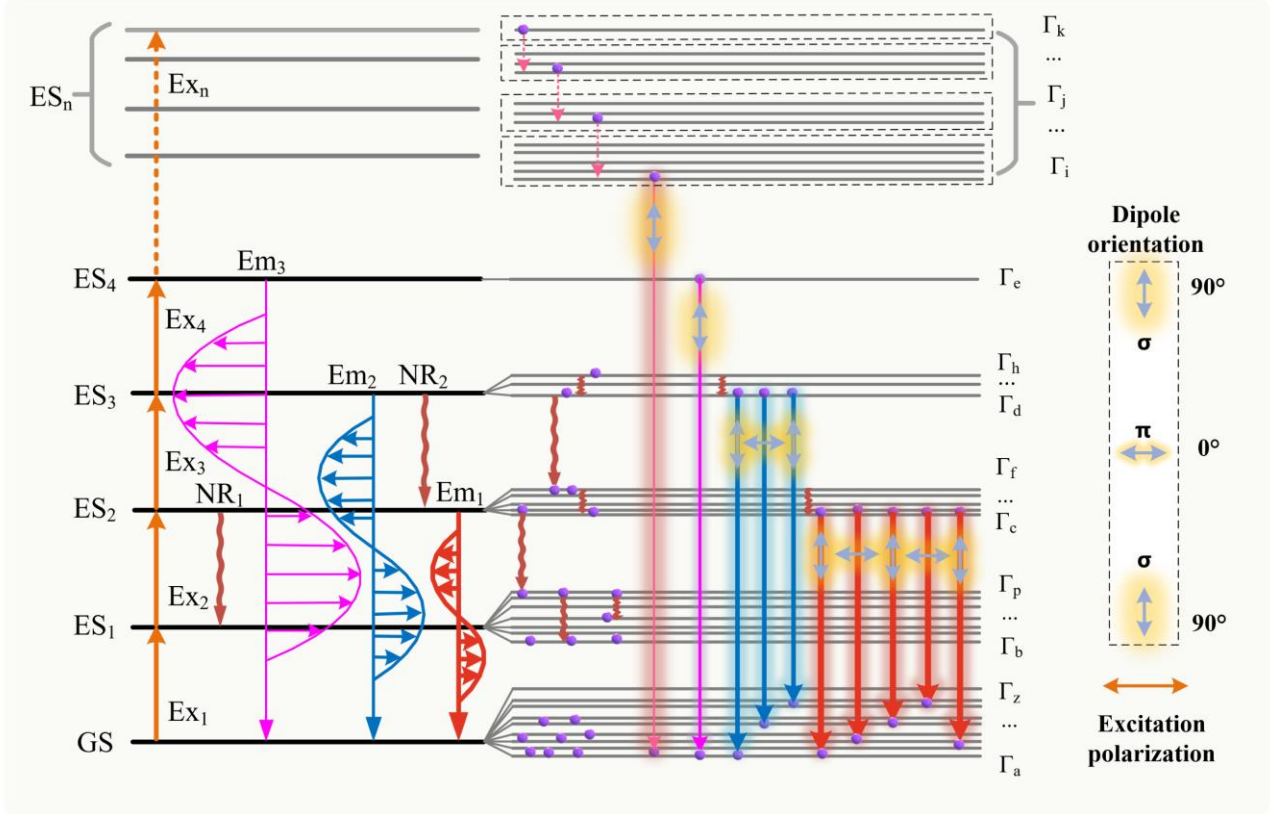


**Figure 1.** Schematic diagram of multiphoton enhancement of DOP of PUCL in  $\text{Ln}^{3+}$  ions.

energy state of  $\text{ES}_4$  pumped by the four-photon upconversion process is greater than the two-photon process, resulting in a lower population density ( $N_4 < N_2$ ). Thus, under the same excited power, the population density of ES with a four-photon process is much smaller than that of a two-photon process. Therefore, we can control the population density of  $\text{ES}_i$  by the number of photons in upconversion processes.

In the hexagonal phase of  $\text{NaYF}_4$ , the  $2s+1L_J$  energy level of  $\text{Ln}^{3+}$  can split into the  $2J+1$  energy level, corresponding to irreducible  $\Gamma_n$  symmetry,<sup>[30,31]</sup> because of the  $C_s$  point group symmetry.<sup>[29]</sup> Irreducible transitions  $\Gamma_d(\text{ES}_3) \rightarrow \Gamma_a(\text{GS})$  ( $d \neq a$ ) generate UCL for the three-photon upconversion process (Figure 1). Among those transitions, some transition dipoles exhibit excitation polarization dependence for dipole orientation. But the dipole orientations might vary from each other, such as  $\sigma$  and  $\pi$  polarization. And the mixed dipole orientations reduce the probability of similar dipole orientations, resulting in a low or canceled PUCL. Thus, the DOP of PUCL depends on mixed irreducible transitions  $\Gamma_d(\text{ES}_3) \rightarrow \Gamma_a(\text{GS})$  with different dipole orientations. Compared with the three-photon upconversion process, the population density of the  $\text{ES}_4$  is lower because of the four-photon upconversion process and the low energy transfer efficiency. And the mixing for different dipole orientations is reduced, which prefers the similar orientation and gives a higher DOP for PUCL. While the population density of the  $\text{ES}_2$  is larger for two-photon upconversion process due to the less photons for UCL. As a result, the possibility of mixed different orientations of dipole transitions increases, and DOP of PUCL is smaller or even disappeared. Therefore, the number of upconversion photons influences the population density of ES and the DOP of PUCL through the irreducible transition  $\Gamma_i(\text{ES}_n) \rightarrow \Gamma_a(\text{GS})$  with different dipole orientations (Figure 1). However, in the traditional upconversion process, the number of upconversion photons and the population density of  $\text{ES}_i$  are also affected by NR transitions such as energy transfer, cross-relaxation, and excitation wavelength. We expect to control the DOP of PUCL through tuning the population density of  $\text{ES}_i$  by the number of upconversion photons, accompanying with the interaction of NR transitions and the excitation wavelength.

## 2.2. Highly polarized $\text{NaYF}_4:\text{Ho}$ upconversion luminescence nanorods.

$\text{Ho}^{3+}$  is first chosen to realize the modulation of DOP by the number of upconversion photons for its excellent photochemical stability and ladder-type energy levels.  $\text{NaYF}_4\text{:Ho}$  nanorods (length  $\approx 1460 \pm 200$  nm, diameter  $\approx 108 \pm 20$  nm) were synthesized by a typical hydrothermal method (Figure S1a-c). And the length of nanorods is greater than the excitation spot diameter (1080 nm) (Figure 2b and Supplementary Section 1). The optical measurement of a single nanorod is realized by a home-built micro-region platform (Figure 2a), where a half-wave plate is placed in the excitation path to change the direction of the electronic field of the excitation light. Under the excitation of an 1150 nm laser, the UCL spectra (Figure 2c) of  $\text{NaYF}_4\text{:Ho}$  single nanorods were obtained. Four emission peaks were presented, centered around 486 nm, 541 nm, 750 nm, and 648 nm, respectively, corresponding to the four transitions of  $\text{Ho}^{3+}$  ions:  $^5\text{F}_3 \rightarrow ^5\text{I}_8$ ,  $^5\text{F}_4/^5\text{S}_2 \rightarrow ^5\text{I}_8$ ,  $^5\text{F}_4/^5\text{S}_2 \rightarrow ^5\text{I}_7$ , and  $^5\text{F}_5 \rightarrow ^5\text{I}_8$ , respectively. Then, PUCL spectra of  $\text{NaYF}_4\text{:Ho}$  single nanorods can be obtained (Figure 2c) by changing the polarization direction of the excitation laser. The luminescence intensities of the four transitions show the same trend with varying polarization angles. All of the transitions appear a period of  $180^\circ$  by fitting the luminescence intensities using the

$$y = y_0 + A * \sin^2(\theta) \quad (2)$$

function (Figure S1d). The DOP is defined as:

$$\text{DOP} = \frac{(I_{\max} - I_{\min})}{(I_{\max} + I_{\min})} \quad (3),$$

where  $I_{\max}$  and  $I_{\min}$  are the maximum and minimum intensities of integrated UCL, respectively. The DOP for four transitions of  $^5\text{F}_3 \rightarrow ^5\text{I}_8$ ,  $^5\text{F}_4/^5\text{S}_2 \rightarrow ^5\text{I}_8$ ,  $^5\text{F}_4/^5\text{S}_2 \rightarrow ^5\text{I}_7$  and  $^5\text{F}_5 \rightarrow ^5\text{I}_8$  are calculated to be 0.859, 0.861, 0.847, and 0.681, respectively. It is interesting that the DOP of  $^5\text{F}_3 \rightarrow ^5\text{I}_8$ ,  $^5\text{F}_4/^5\text{S}_2 \rightarrow ^5\text{I}_8$ , and  $^5\text{F}_4/^5\text{S}_2 \rightarrow ^5\text{I}_7$  transitions are close to each other, which are larger than the transition of  $^5\text{F}_5 \rightarrow ^5\text{I}_8$ . According to the relationship between the DOP and the number of upconversion photons, this phenomenon implies that the number of upconversion photons for  $^5\text{F}_3 \rightarrow ^5\text{I}_8$ ,  $^5\text{F}_4/^5\text{S}_2 \rightarrow ^5\text{I}_8$ , and  $^5\text{F}_4/^5\text{S}_2 \rightarrow ^5\text{I}_7$  transitions is consistent and larger than the number of photons for the  $^5\text{F}_5 \rightarrow ^5\text{I}_8$  transition.

The excitation power dependence of a single nanorod is carried out to assess the upconversion process (Figure 2d and Figure S1e). The number of photons ( $n$ ) required to populate the emitting state can be calculated by the relation between:

$$I_{em} \propto P^n \quad (4),$$

where  $I_{em}$  is the integral intensity of UCL and  $P$  is the pump power of the laser.<sup>[34]</sup>  $n_1 = 1.90$ , which corresponds to the  $^5\text{F}_5 \rightarrow ^5\text{I}_8$  transition, indicating that two photons are required to pump the  $^5\text{F}_5$  state.  $n_2$ ,  $n_3$ , and  $n_4$  for the three transitions of  $^5\text{F}_4/^5\text{S}_2 \rightarrow ^5\text{I}_7$ ,  $^5\text{F}_4/^5\text{S}_2 \rightarrow ^5\text{I}_8$ , and  $^5\text{F}_3 \rightarrow ^5\text{I}_8$  are 2.20, 2.32, and 2.44, respectively, suggesting the three-photon upconversion process. Thus, the DOP of the transitions with three-photon pumping is larger than that of the transition with a two-photon process (Figure 2e). This verifies our strategy to regulate the polarized luminescence based on the number of upconversion photons. The greater the number of upconversion photons, the smaller the population density of ESs, and the higher the DOP of PUCL.

The DOPs of different transitions are regulated by the population density of ESs. In the typical multiphoton upconversion transition process of  $\text{Ho}^{3+}$  excited at 1150 nm (Figure 2f),  $^5\text{F}_3 \rightarrow ^5\text{I}_8$ ,  $^5\text{F}_4/^5\text{S}_2 \rightarrow ^5\text{I}_8$ ,  $^5\text{F}_4/^5\text{S}_2 \rightarrow ^5\text{I}_7$  are three-photon upconversion processes, and  $^5\text{F}_5 \rightarrow ^5\text{I}_8$  is a two-photon upconversion process, where the ESs of  $^5\text{F}_4/^5\text{S}_2$  originate from the NR transition of the  $^5\text{F}_3$  state. Any transition is a mixture of irreducible transitions  $\Gamma_n$  (ES)  $\rightarrow \Gamma_m$  (GS) with various dipole orientations.<sup>[35]</sup> Compared with the three-photon process, the two-photon process has a larger population density of ES, thus the mixing probability of different dipole orientations in the two-photon process is much larger than that of the three-photon process, resulting in a lower DOP. Those phenomena are consistent with our proposed regulation strategy, indicating the DOP of PUCL can be adjusted by modulating the population density of ESs.

Furthermore, the population density of ES can be controlled by the pump power of the excited source, thus, the DOP of PUCL can be operated by the pump power density of the excitation light. Since the relationship:

$$N_i \propto P^n \quad (5),$$

where  $N_i$  is the population density of ESs and  $P$  is excited power,<sup>[36]</sup> the population density of ES  $N_i$  will increase if enhancing the excited power  $P$ . Here, the statistics of DOP from a single nanorod on excited power are presented (Figure 2g). It is found that

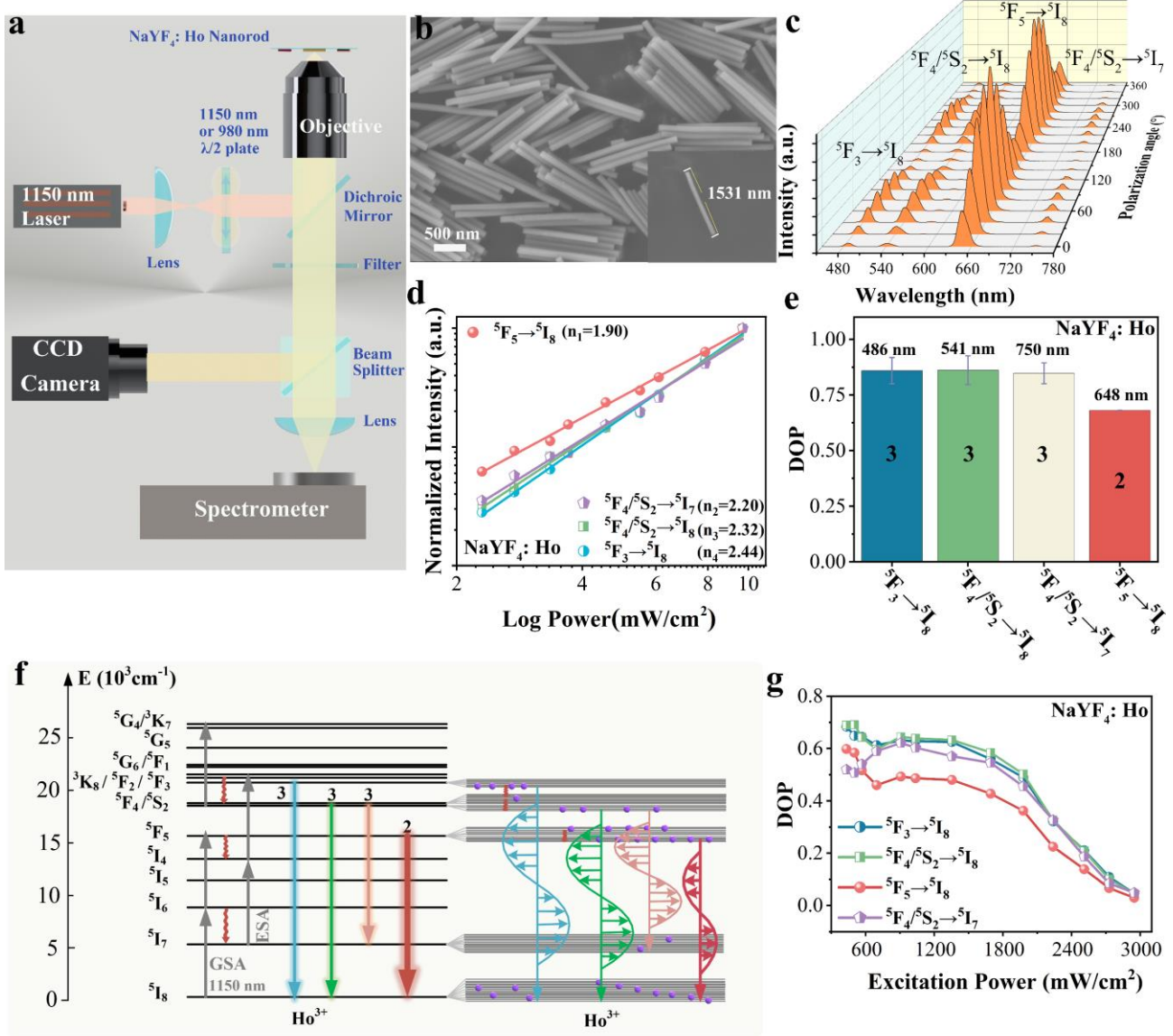


**Figure 2.** a) Schematic illuminated the UCL of NaYF<sub>4</sub>:8% Ho single nanorods, which were collected by a home-built optical microscope system. b) Scanning electron microscope (SEM) image of NaYF<sub>4</sub>:8% Ho nanorods; the inset is the single nanorod. c) PUCL spectra of a NaYF<sub>4</sub>:8% Ho single nanorod excited at 1150 nm. d) Normalized intensities of a NaYF<sub>4</sub>:8% Ho single nanorod as a function of excitation power at 1150 nm. e) Histogram illustrated the photon number connected DOPs of four transitions. f) Schematic diagram of the multiphoton upconversion mechanism of Ho<sup>3+</sup> excited at 1150 nm, accompanying the population density of ES<sub>i</sub> and DOPs of different transitions. g) Dependence of the DOP on the pump power density of the excitation light.

the DOPs are decreased for all of the upconversion transitions. But the DOPs from three-photon transitions are also kept higher than that from two-photon transition at any power. Moreover, the DOPs are reduced to 0 for all the transitions, and PUCL are disappeared accompanying with much enhanced UCL intensity when the power is large enough. This is because ESs of the four transitions are close to saturation when high power,<sup>[36]</sup> inducing strong mixing of different dipole orientations from irreducible transitions  $\Gamma_m$  (ES)  $\rightarrow$   $\Gamma_n$  (GS) for any emission bands. Hence, the UCL is depolarized. The diminished trend of DOPs with increasing power expresses that a saturated population of ESs suppresses the PUCL from Ln<sup>3+</sup>. Furthermore, the population density of ES can dominate the DOP, which verifies the polarization strategy regulated by the number of upconversion photons.

### 2.3. Cross-relaxation and the number of upconversion photons tune the DOPs of PUCL.

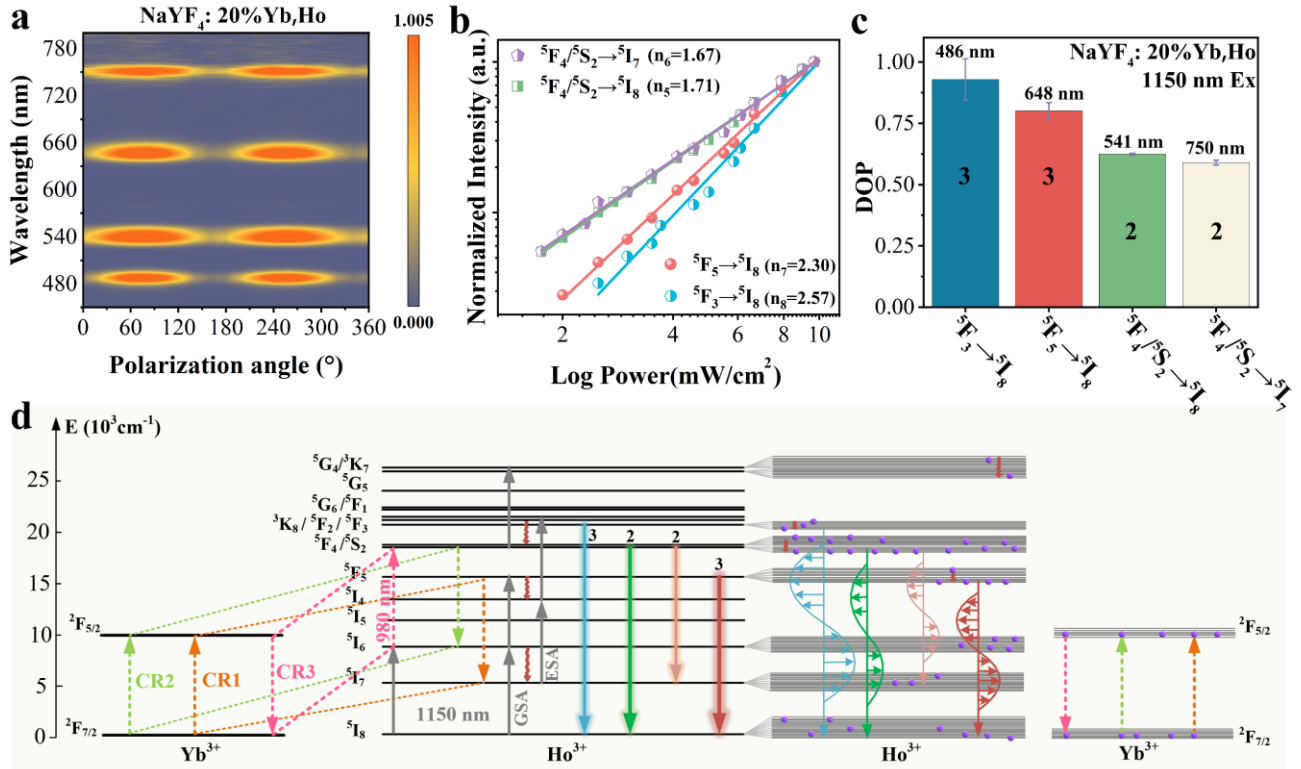


**Figure 3.** a) Matrix diagram of PUCL from NaYF<sub>4</sub>:20% Yb,8% Ho single nanorod excited by 1150 nm. b) Excitation power dependence of emission dynamics. c) Histogram illustrated the photon number connecting DOPs of four transitions. d) Schematic illustration of the multiphoton upconversion of NaYF<sub>4</sub>:Yb,Ho excited at 1150 nm.

The number of upconversion photons and the population density of ES are also affected by NR transitions such as cross-relaxation. The DOP strategy based on the number of upconversion photons is still effective with cross-relaxation. Here, we introduced cross-relaxation between Yb<sup>3+</sup> and Ho<sup>3+</sup> to monitor the DOPs from Ho<sup>3+</sup> (Figure S2a-c). The same emission peaks are detected under 1150 nm excitation (Figure S3a), and PUCL also exhibits a periodic change of 180° with changing the polarization angle of the excitation light (Figure 3a and Figure S3d). On the one hand, the DOPs are 0.623 and 0.590 for the two-photon transitions  $^5F_4/^5S_2 \rightarrow ^5I_8$  and  $^5F_4/^5S_2 \rightarrow ^5I_7$ , respectively (Figure 3b,c and Figure S4a). Both of the transitions come from the same ESs of  $^5F_4/^5S_2$  and present similar DOPs. On the other hand, the DOPs are 0.800 and 0.929 for the three-photon transitions  $^5F_5 \rightarrow ^5I_8$  and  $^5F_3 \rightarrow ^5I_8$ , respectively (Figure 3b,c and Figure S4a). Obviously, the DOPs of two-photon transitions are significantly smaller than those of three-photon transitions, which is consistent with the polarization strategy regulated by the number of upconversion photons. It is interesting that the  $^5F_4/^5S_2 \rightarrow ^5I_8$  and  $^5F_4/^5S_2 \rightarrow ^5I_7$  transitions are two-photon processes in NaYF<sub>4</sub>:Yb,Ho single nanorod, while those are three-photon processes in NaYF<sub>4</sub>:Ho single nanorod, indicating different pump paths for the same transitions.

The anomalous upconversion path for  $^5F_4/^5S_2 \rightarrow ^5I_8$  and  $^5F_4/^5S_2 \rightarrow ^5I_7$  transitions is originated from cross-relaxation between Yb<sup>3+</sup> and Ho<sup>3+</sup> when introducing Yb<sup>3+</sup> into nanorods and excited by 1150 nm (Figure 3d and Figure S4b-e). The  $^5F_4/^5S_2$  states are come from the GSA of 1150 nm to  $^5I_6$  metastable state, followed by the cross-relaxation (CR3)  $^5I_6$  (Ho<sup>3+</sup>) +  $^2F_{5/2}$  (Yb<sup>3+</sup>)  $\rightarrow$   $^5F_4/^5S_2$  (Ho<sup>3+</sup>) +  $^2F_{7/2}$  (Yb<sup>3+</sup>) (Figure 3d and Figure S4).<sup>[37]</sup> Hence, the  $^5F_4/^5S_2 \rightarrow ^5I_8$  and  $^5F_4/^5S_2 \rightarrow ^5I_7$  transitions become a two-photon upconversion process in a Yb<sup>3+</sup> co-doped single nanorod from a three-photon process in a Ho<sup>3+</sup> mono-doped single nanorod. For the same transition from  $^5F_4/^5S_2$  states, three-photon upconversion pumps a lower population density and gives a higher DOP of PUCL compared with the two-photon process. Those results show that the DOPs of PUCL are mainly determined by population density in ESs and not the energy levels themselves.

#### 2.4. Excitation wavelength regulates DOPs of PUCL.



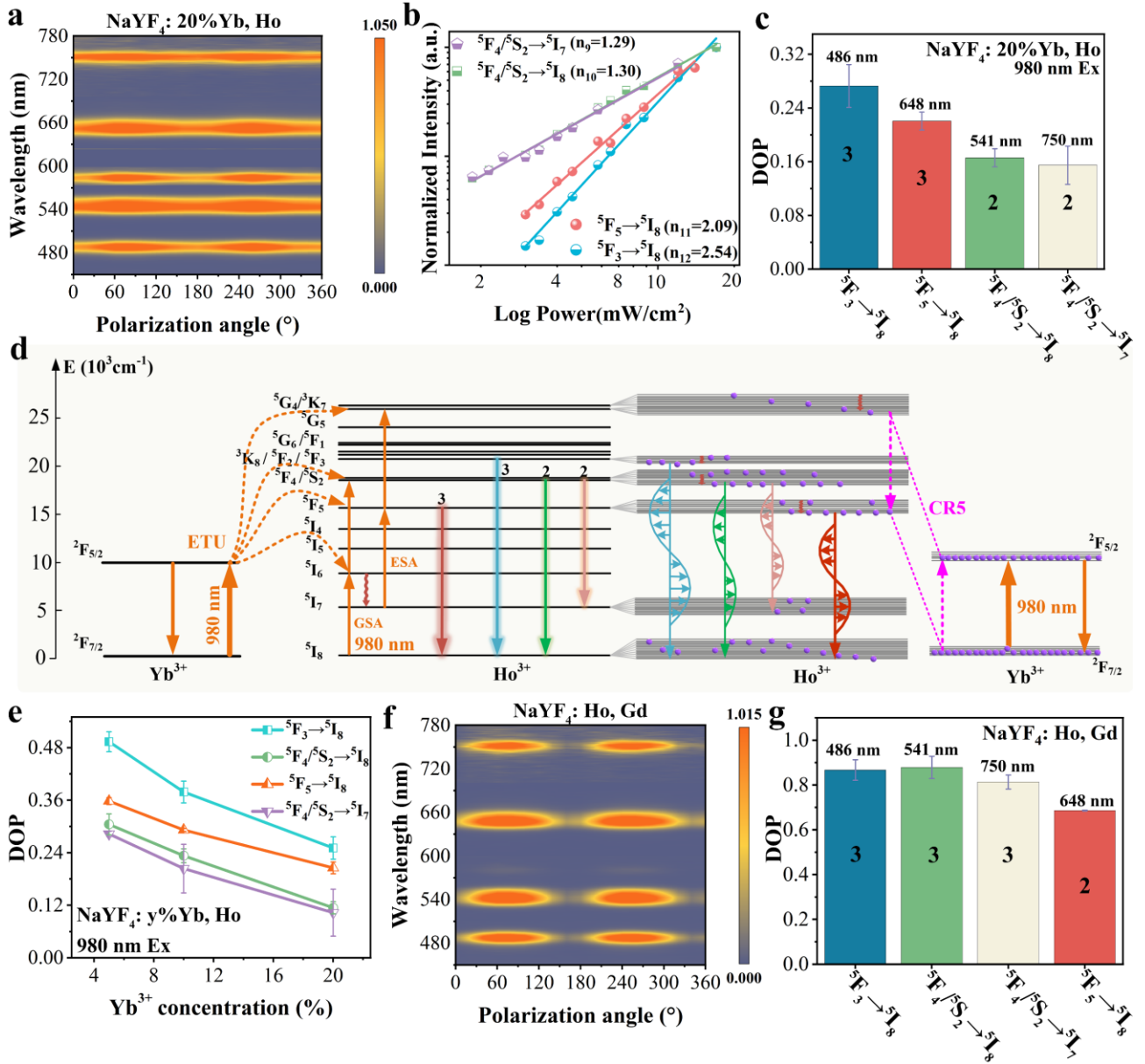


**Figure 4.** a) Matrix diagram of UCL spectra from NaYF<sub>4</sub>:20% Yb,8% Ho single nanorod excited at 980 nm. b) Excitation power dependence of emission dynamics. c) Histogram illustrated the photon number connected DOPs of four transitions. d) Schematic illustration of the multiphoton upconversion mechanism of NaYF<sub>4</sub>:Yb,Ho excited at 980 nm, accompanying with DOPs regulated by the number of upconversion photons. e) The DOPs of four transitions depend on the concentration of Yb<sup>3+</sup>. f) Matrix diagram of UCL spectra from NaYF<sub>4</sub>:10% Gd,8% Ho single nanorod excited at 1150 nm. g) Histogram illustrated the photon number connected DOPs of four transitions from Gd<sup>3+</sup> co-doped single nanorod excited at 1150 nm.

The number of upconversion photons is correlated to the wavelength of the excitation light. Generally speaking, for the same ES, the number of required upconversion photons with high energy is less than that with low energy because of the different pumping path. We changed the excitation wavelength to 980 nm to vary the pump path and regulate DOP (Figure 4a and Figure S5a,d). DOPs for two-photon transitions  $^5F_4/^5S_2 \rightarrow ^5I_8$  and  $^5F_4/^5S_2 \rightarrow ^5I_7$  are 0.166 and 0.155, respectively. And DOPs for three-photon process  $^5F_5 \rightarrow ^5I_8$  and  $^5F_3 \rightarrow ^5I_8$  transitions are 0.221 and 0.273, respectively (Figure 4b,c and Figure S6a). The greater the number of photons required, the higher the DOPs of UCL, which is consistent with our proposed strategy of controlling the DOP by the number of photons. In addition, DOP of  $^5F_5 \rightarrow ^5I_8$  transition is smaller than that of  $^5F_3 \rightarrow ^5I_8$  transition, although the same number of required photons for  $^5F_5 \rightarrow ^5I_8$  and  $^5F_3 \rightarrow ^5I_8$  transitions.

The difference is derived from the various pump channels. The  $^5F_5$  state comes from two paths. One way is the general two-photon upconversion process. The other way is the three-photon process with cross-relaxation (CR5):  $^5G_4/{}^3K_7 (Ho^{3+}) + {}^2F_{7/2} (Yb^{3+}) \rightarrow {}^5F_5 (Ho^{3+}) + {}^2F_{5/2} (Yb^{3+})$  (Figure 4d and Figure S4c). While  $^5F_3$  state is pumped by three-photon absolutely. Thus, the population density of the  $^5F_5$  state is higher than that of the  $^5F_3$  state, resulting in a lower DOP for the  $^5F_5 \rightarrow {}^5I_8$  transition.

The population density of ESs is also tuned by the synergistic effect of the excitation wavelength and  $Yb^{3+}$  doping based on the number of upconversion photons. As  $Yb^{3+}$  concentration increases, the population density of ESs will have a significant increment because of the larger absorption cross of  $Yb^{3+}$  and enhanced energy transfer from  $Yb^{3+}$  to  $Ho^{3+}$  (Figure S5 and S6b).<sup>[38]</sup> The higher population density of ESs can induce a strong mixing of different dipole orientations and lead to a low DOP (Figure 4e). Indeed, with the same number of upconversion photons, the DOPs are 0.221 and 0.273 for  $^5F_5 \rightarrow {}^5I_8$  and  $^5F_3 \rightarrow {}^5I_8$  transitions (Figure 4c), respectively, in a  $Yb^{3+}$  co-doped single nanorod excited at 980 nm, while they are 0.800 and 0.929 in the same single nanorod excited at 1150 nm (Figure 3c). The same situation exists for two-photon  $^5F_4/{}^5S_2 \rightarrow {}^5I_8$  and  $^5F_4/{}^5S_2 \rightarrow {}^5I_7$  transitions (Figure 4c and Figure 3c). The remarkable reduction of DOPs from the  $Yb^{3+}$  co-doped single nanorod reconfirms the regulated strategy of ESs population density and the number of upconversion photons.

The regulated strategy based on the number of upconversion photons keeps working with the changing local site symmetry around activators. It has been reported that the bonding length and bonding angles between  $Ln^{3+}$  and  $F^-$  are altered with co-doped  $Gd^{3+}$  in nanorods, which changes the local symmetry and polarized behavior of  $Ln^{3+}$ .<sup>[1,39]</sup> In this section, we introduced a high concentration of  $Gd^{3+}$  ions into  $Ho^{3+}$ -doped nanorods (Figure 4f and Figure S7a). The DOPs for  $^5F_3 \rightarrow {}^5I_8$ ,  $^5F_4/{}^5S_2 \rightarrow {}^5I_8$ , and  $^5F_4/{}^5S_2 \rightarrow {}^5I_7$  transitions are 0.867, 0.878, and 0.814 (Figure 4g), which are three-photon upconversion processes (Figure S7b,c). And the DOP for the  $^5F_5 \rightarrow {}^5I_8$  transition is 0.686 (Figure 4g), which is a two-photon upconversion process (Figure S7b,c). Notably, the DOPs of three-photon upconversion are higher than those of the two-photon process. Thus, the presented performance is in line with the regulated strategy.

## 2.5. Tunable DOPs of PUCL from $Tm^{3+}$ are based on the number of upconversion photons.

The regulated strategy of DOPs based on the number of upconversion photons can be extended to  $Tm^{3+}$  because of the excellent ladder-type energy levels required to realize multiphoton upconversion.<sup>[32]</sup> The UCL spectra from a  $NaYF_4:Tm,Yb$  single nanorod (Figure 5a) present five emission bands upon excitation at 980 nm (Figure 5b). The emission bands are centered around 452 nm, 476 nm, 648 nm, 695 nm, and 792 nm, respectively, corresponding to  ${}^1D_2 \rightarrow {}^3F_4$ ,  ${}^1G_4 \rightarrow {}^3H_6$ ,  ${}^1G_4 \rightarrow {}^3F_4$ ,  ${}^3F_3 \rightarrow {}^3H_6$ , and  ${}^3H_4 \rightarrow {}^3H_6$  transitions of  $Tm^{3+}$ . Then, the luminescence intensity was normalized by the deconvolution method and fitted by the

$$y = y_0 + A * \sin^2(\theta) \quad (2)$$

function (Figure 5c). It is found that three kinds of DOPs are presented, corresponding to different upconversion modes. First is the two-photon upconversion path (Figure 5d and Figure S7d), and the DOPs of the  ${}^3F_3 \rightarrow {}^3H_6$  and  ${}^3H_4 \rightarrow {}^3H_6$  transitions are 0.233 and 0.275, respectively (Figure 5e). The second is the three-photon upconversion way (Figure 5d), and the DOPs of the  ${}^1G_4 \rightarrow {}^3H_6$  and  ${}^1G_4 \rightarrow {}^3F_4$  transitions are 0.580 and 0.531, respectively (Figure 5e). The third is the four-photon upconversion process (Figure 5d), and the DOP of the  ${}^1D_2 \rightarrow {}^3F_4$  transition is 0.925 (Figure 5e). Evidently, the DOP for the four-photon process is larger than that for the three-photon process. Furthermore, the DOPs from the three-photon process are much greater than those from the two-photon process. Those phenomena are highly coincident with the population density of ESs controlled by upconversion photons. In other words, the more photons required in the upconversion process, the lower the population density of ES (Figure 5f). As a result, the fewer different dipole orientations that mix, the higher the DOP of UCL. It is worth noting that a huge span of DOP from 0.925 to 0.233 is successfully achieved in  $Tm^{3+}$ , which is attributed to the large difference in population density in ESs based on four-photon and two-photon paths.

The modulation of DOPs from  $Tm^{3+}$  UCL can also be realized by the adjustment of population density in ESs by power density of the excitation light. The population density in ESs of  $Tm^{3+}$  increases with increasing pump power of the excitation light, leading



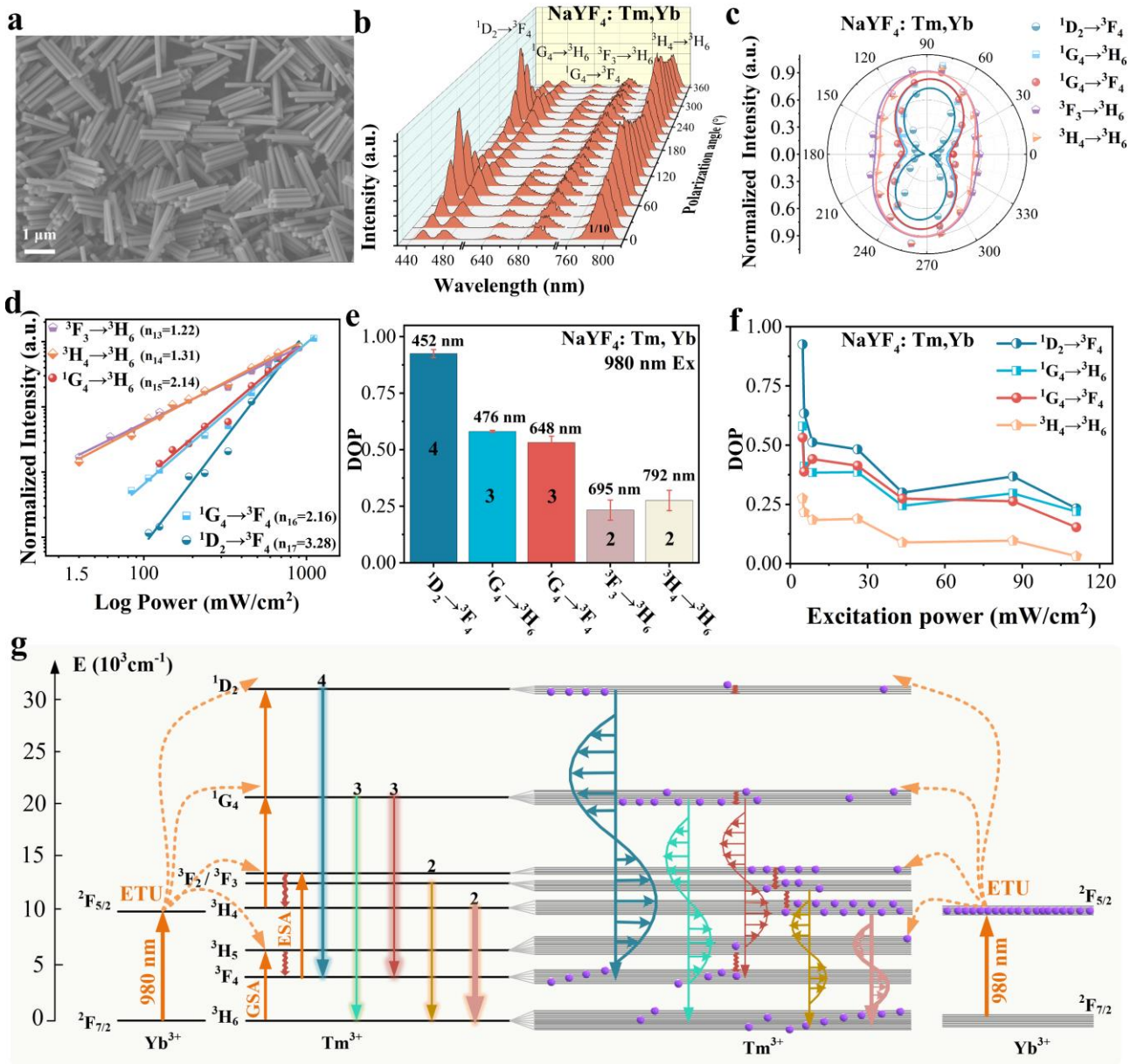


**Figure 5.** a) SEM image of NaYF<sub>4</sub>:5% Tm, 20% Yb nanorods. b) PUCL spectra from NaYF<sub>4</sub>:Yb,Tm single nanorod excited at 980 nm. c) Polar plots the UCL integral intensities from  $^1D_2 \rightarrow ^3F_4$ ,  $^1G_4 \rightarrow ^3H_6$ ,  $^1G_4 \rightarrow ^3F_4$ ,  $^3F_3 \rightarrow ^3H_6$ ,  $^3H_4 \rightarrow ^3H_6$  transitions as a function of the excitation polarization angle. d) Normalized intensities as a function of excitation power at 980 nm. e) Histogram illustrated the photon number connected DOPs of five transitions. f) DOPs of different transitions as a function of excitation power density. g) Energy level diagram of the energy transfer from Yb<sup>3+</sup> to Tm<sup>3+</sup>, accompanied by the DOPs based on the number of upconversion photons.

to an obvious reduced trend of DOPs for all of the emissions (Figure 5f). For the ES  $^1D_2$ , which is originated from four-photon pump way (Figure 5d), the population density is added rapidly with enhancing the excitation power. Then, a mixture of irreducible transitions  $\Gamma_n(^1D_2) \rightarrow \Gamma_m(^3F_4)$  with opposite dipole orientations is raised, resulting in a low proportion for similar dipole orientation and a small DOP of PUCL (Figure 5g). Those are analogous to the transitions of  $^1G_4 \rightarrow ^3H_6$ ,  $^1G_4 \rightarrow ^3F_4$ ,  $^3F_3 \rightarrow ^3H_6$ , and  $^3H_4 \rightarrow ^3H_6$ . Moreover, the reduced trend of DOP for the four-photon transition  $^1D_2 \rightarrow ^3F_4$  is more sensitive than that for the three-photon transitions  $^1G_4 \rightarrow ^3H_6$  and  $^1G_4 \rightarrow ^3F_4$ . And three-photon transitions are fast than two-photon transition  $^3H_4 \rightarrow ^3H_6$ . Therefore, the upconversion photons number regulated population density of ESs can be feedbacked by the DOPs from single nanorod and verified on Tm<sup>3+</sup> and Ho<sup>3+</sup>.

## 2.6. Multi-dimensional polarized anti-counterfeiting display and encryption.

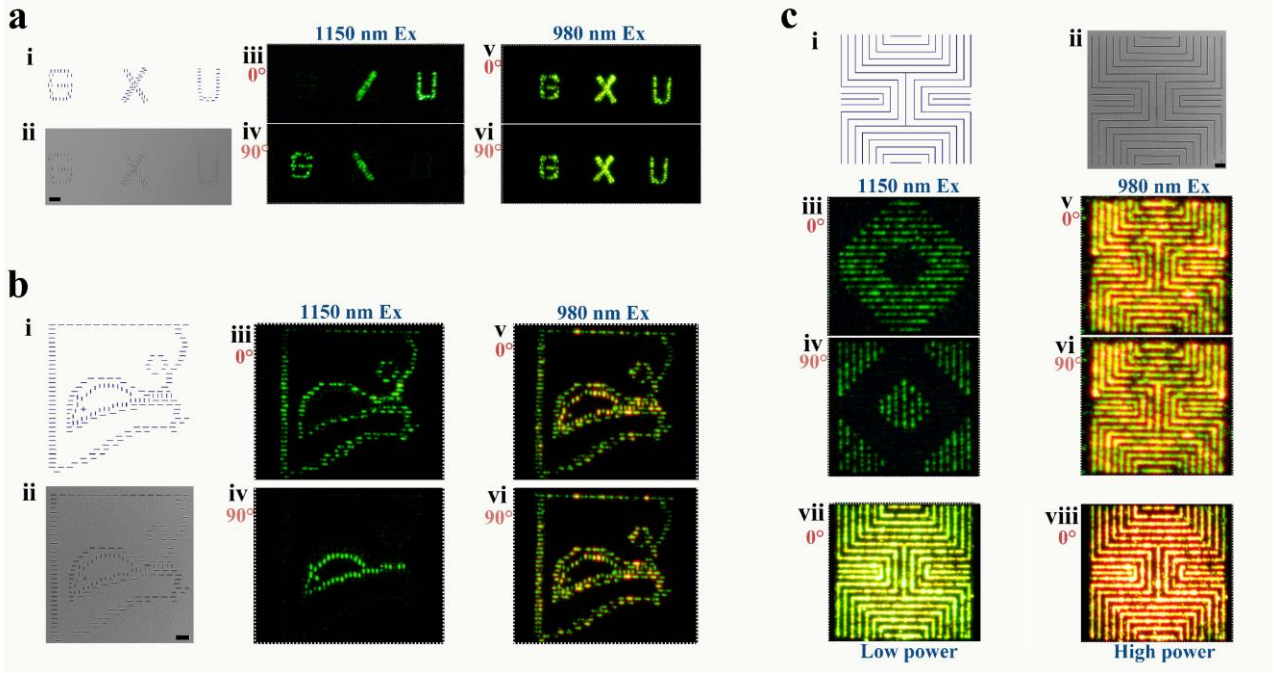


**Figure 6.** a) Design (i) and SEM (ii) images of "G", "X", and "U" letters composed of NaYF<sub>4</sub>:Ho,Yb nanorods, where the pixels of "G" are arranged vertically; the left slashes of "X" ("/") are arranged vertically, and the right slashes ("\") are arranged horizontally; the pixels of "U" are arranged horizontally. Upconversion photoluminescence images of "G", "X", and "U" letters are excited by 1150 nm (iii-iv) or 980 nm (v-vi) with a polarized angle of 0° and 90°. b) Design (i) and SEM (ii) images of "Cat" and "Mouse" patterns composed of NaYF<sub>4</sub>:Ho,Yb nanorods, where "Cat" is composed of a horizontal pixel arrangement and "Mouse" is composed of a vertical pixel arrangement; upconversion photoluminescence images of "Cat" and "Mouse" patterns excited by 1150 nm (iii-iv) or 980 nm (v-vi) with polarized angles at 0° and 90°. c) Design (i) and SEM (ii) images of "Labyrinth Totems" composed of NaYF<sub>4</sub>:Ho,Yb nanorods, in which the vertical nanowire groove is arranged by vertical nanorods, and the horizontal nanowire groove is arranged by horizontal nanorods. Upconversion photoluminescence images of the "Labyrinth Totem" are excited by 1150 nm (iii-iv) or 980 nm (v-vi) with a polarized angle of 0° and 90°. Upconversion photoluminescence images of the "Labyrinth Totem" were excited by 980 nm with a low (vii) and high (viii) power, respectively. All scale bars are 10  $\mu$ m.

The polarized luminescence of single nanorods is able to be applied in anti-counterfeiting displays with multi-dimensional encryption. Here, we introduce an encryption key by polarized luminescence for anti-counterfeiting displays with full use of the low and high DOPs of NaYF<sub>4</sub>:Yb, Ho nanorods upon excitation at 980 nm and 1150 nm, respectively. The low DOP excited by 980 nm can ensure the whole display of all the patterns, while the high DOP excited by 1150 nm is able to present the detail pictures, which provides an excellent opportunity for us to customize related patterns as polarized anti-counterfeiting displays. In detail, a rectangular groove is etched in a silicon wafer as the pixel point for patterns by electron beam lithography (EBL) and reactive ion etching (RIE) (Figure S8a). The width of the groove is less than the length of a single nanorod (Figure S8b), thus, nanorods can only be filled into the grooves along the rectangular groove (Figure S8c,d). By software design, the rectangular groove can be arranged into any pattern with an arbitrary size according to the designer's idea. Thus, we can consider the rectangular groove as a pixel point.

"G", "X", and "U" letters were first etched and filled by NaYF<sub>4</sub>:Yb, Ho nanorods (Figure 6a). The "G" and "U" are arranged by vertical and horizontal nanorods, respectively. "X" is arrayed by vertical ("/") and horizontal ("\") nanorods, respectively. Upon excitation at 1150 nm with a polarization angle of 0°, "U" and "/" of "X" letters are illuminated, while "\ of "X" and "G" letters are hidden (Figure 6a-iii). When we changed the angle to 90°, "\ of "X" and "G" letters were displayed, while "U" and "/" of "X"

letters disappeared (Figure 6a-iv). At the same time, the whole letters "G", "X", and "U" can be completely shown under excitation at 980 nm due to the low DOP of nanorods (Figure 6a-v and 6a-vi). Therefore, selective encryption and display can be realized by using different excitation wavelengths.

Graph encryption can be extended following the letter's encryption (Figure 6b). The "Cat" and "Mouse" profiles are etched, where the "Cat" and "Mouse" are filled by horizontal and vertical nanorods, respectively. We can see the "Mouse" patterns when excitation is at 1150 nm and 0° of polarized angle (Figure 6b-iii). While changing the polarized angle to 90°, the "Cat" graph is presented (Figure 6b-iv). In addition, when excited at 980 nm, the "Cat" and "Mouse" pictures appear simultaneously regardless of the polarization angle of the excitation source (Figure 6b-v and 6b-vi). These horizontal and vertical designs not only perform excellently in the encryption and hiding of words but also present a brilliant performance in the anti-counterfeiting encryption of pictures.

Furthermore, a high-polarized signal can be achieved in a "Labyrinth Totem" composed of vertical and horizontal nanowire grooves (Figure 6c). The width of a nanowire groove is also much smaller than the length of NaYF<sub>4</sub>:Yb, Ho nanorods; thus, the nanorods can only be arrayed along the direction of nanowire grooves (Figure S8e). Upon excitation at 1150 nm and 0° of polarized angle, a hollow diamond is presented (Figure 6c-iii). While it is disappeared when excited at 90° of polarized angle (Figure 6c-iv). Meanwhile, the whole "Labyrinth Totem" is illuminated when excited by 980 nm with an orange color (Figure 6c-v and 6c-vi). Besides, the green (Figure 6c-vii) and red (Figure 6c-viii) colors of the whole "Labyrinth Totem" emerge during excitation at 980 nm with a low and high power, respectively. Finally, five-fold anti-counterfeiting is achieved. Our design provides multiple guarantees for anti-counterfeiting displays and opens up infinite possibilities for polarized luminescence in designable patterns and multi-dimensional anti-counterfeiting displays.

### 3. Conclusions

In summary, we demonstrate a strategy to regulate the DOPs of PUCL from Ln<sup>3+</sup>-doped single nanorods based on the number of upconversion photons. The core of this strategy is the population density of ESs tuned by the number of upconversion photons. Compared with the two-photon ESs, population density of ESs, which required much more photons, is lower. The lower population density generates a higher possibility for similar dipole orientation and a larger DOP of PUCL. The modulation of the DOPs of PUCL from Ho<sup>3+</sup> and Tm<sup>3+</sup> is realized by cross-relaxation, excitation wavelength, power density, and changed local site symmetry. The DOPs has been controlled from 0.233 of two-photon upconversion process to 0.925 of four-photon upconversion process in Tm<sup>3+</sup>. Besides, by taking advantage of the highly polarized nature of a single nanorod, multi-dimensional anti-counterfeiting display and encryption in words, pictures, and a labyrinth totem have been realized. This regulated polarization strategy will promote the development of PUCL from Ln<sup>3+</sup>. The tunable polarization properties combined with multi-dimensional encryption methods enable potential applications in three-dimensional display, optical encoding, and many other emerging fields.

### 4. Experimental Section

**Chemicals and reagents.** All chemicals and solvents were obtained from commercial sources without further purification. NH<sub>4</sub>F (99.99%), NaOH (99.99%), Y(NO<sub>3</sub>)<sub>3</sub>·6H<sub>2</sub>O (99.99%), Yb(NO<sub>3</sub>)<sub>3</sub>·6H<sub>2</sub>O (99.99%), Ho(NO<sub>3</sub>)<sub>3</sub>·6H<sub>2</sub>O (99.99%), Tm(NO<sub>3</sub>)<sub>3</sub>·6H<sub>2</sub>O (99.99%), and oleic acid (90%) were purchased from Sigma-Aldrich (St Louis, MO, USA). Ethanol, cyclohexane, and silicon wafers were purchased from Aladdin. E-Beam Resist PMMA 950K was purchased from ALLRESIST (German Tech Co., Ltd.).

**Synthesis of NaYF<sub>4</sub> nanorods.** Lanthanide-doped nanoparticles were synthesized as described in a previous report.<sup>[40]</sup> NaYF<sub>4</sub> nanorods were synthesized by a hydrothermal method. In the typical synthesis of NaYF<sub>4</sub> nanorods, NaOH (0.3 g) was first dissolved in deionized water (1.5 mL) by adding oleic acid (5 mL) and ethanol (5 mL) as additives under continuous stirring.

Then,  $\text{NH}_4\text{F}$  (2 M, 1 mL) was added to form a turbid mixture. Subsequently,  $\text{RE}(\text{NO}_3)_3$  ( $\text{RE} = \text{Y, Yb, Ho, or Tm}$ ) (0.2 M, 2 mL) was poured into the mixture. After being stirred for 20 minutes, the mixture was transferred to a 50 mL stainless steel Teflon-lined autoclave and kept at 220 °C for 12 hours in an oven. The nanorods were collected by centrifugation and washed with ethanol and cyclohexane three times. Finally, the nanorods were dried at 60 °C for 6 hours before use.

**Field emission scanning electron microscope characterization.** SEM images were obtained from a ZEISS Sigma-500 field emission scanning electron microscope. Energy dispersive spectrum (EDS) characterization was performed using a ZEISS Sigma-500 and an EDS detector (Oxford X-MaxN20) operated at an acceleration voltage of 15 kV.

**Testing of polarized upconversion luminescence from single nanorod.** To measure the PUCL from lanthanide-doped  $\text{NaYF}_4$  single nanorods, a home-built optical microscope system (Figure 2a) was used: an external optical path was used to introduce 1150 nm (or 980 nm) linearly polarized light as the excited light source into an Olympus IX73 inverted microscope, which was coupled with an Edinburgh FLS1000 spectrometer. A half-wave plate at 1150 nm (or 980 nm) was placed in the path of the excited light. Photoluminescence spectra were recorded at room temperature using a FLS1000 spectrometer (Edinburgh Instruments) equipped with an PMT-900 photon-counting photomultiplier tube, and the PUCL spectra were obtained by rotating the half-wave plate.

**Display template manufacturing and nanorods assembly** (Figure S8a). The positive e-beam resist of polymethyl methacrylate (PMMA) was spun onto the substrate of a silicon wafer with 300 nm silicon oxide at 4000 rpm for 60 s. Then the substrate was baked at 180 °C for 2 minutes. Following etched by EBL (RAITH ELPHY & ZEISS-SEM) at 10 KV acceleration voltage and 80 pA beam current. The etched patterns were immersed in a developer solution of methyl isobutyl ketone and isopropanol (IPA) (1:3) for 30 seconds and then flushed with IPA to present the patterns. Then, the patterns were etched by RIE (TEGAL 903E). Finally, the patterns with the pixel point of the rectangle groove were built. The nanorods were assembled in rectangular grooves by polydimethylsiloxane (PDMS). The nanorods, dispersed in ethanol, were dripped on the substrate, which was dragged across the surface several times using PDMS at a speed of 0.5 mm/s (Figure S8d).

## Supplementary Information

Supporting Information is available from the Wiley Online Library or from the author.

## Acknowledgments

The work is supported by National Natural Science Foundation of China (No. 11704081, 52125205, 52250398, U20A20166, 52192614 and 52003101 ), the Guangxi Natural Science Foundation (Nos. 2020GXNSFAA297182, 2020GXNSFAA297041, and 2017GXNSFBA198229), the special fund for "Guangxi Baigui Scholars", National key R&D program of China (2021YFB3200302 and 2021YFB3200304), Natural Science Foundation of Beijing Municipality (2222088), Shenzhen Science and Technology Innovation Program (Grant No. KQTD20170810105439418) and the Fundamental Research Funds for the Central Universities.

## Conflict of Interest

The authors declare no conflict of interest.

## Data Availability Statement

The data that support the findings of this study are available from the corresponding author upon reasonable request.

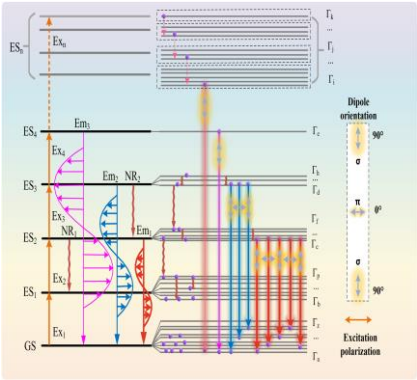
## References

- [1] J. Zhou, G. Chen, E. Wu, G. Bi, B. Wu, Y. Teng, S. Zhou, J. Qiu, *Nano Lett.* **2013**, *13*, 2241.
- [2] T. Hu, Y. Gao, M. S. Molokeev, Z. Xia, Q. Zhang, *Adv. Opt. Mater.* **2021**, *9*, 2100077.
- [3] S. Wei, X. Shang, P. Huang, W. Zheng, E. Ma, J. Xu, M. Zhang, D. Tu, X. Chen, *Sci. China Mater.* **2021**, *65*, 220.
- [4] B. Zhou, B. Shi, D. Jin, X. Liu, *Nat. Nanotechnol.* **2015**, *10*, 924.
- [5] C. Chen, D. Jin, *Nat. Photonics* **2022**, *16*, 553.
- [6] X. Liu, H. Chen, Y. Wang, Y. Si, H. Zhang, X. Li, Z. Zhang, B. Yan, S. Jiang, F. Wang, S. Weng, W. Xu, D. Zhao, J. Zhang, F. Zhang, *Nat. Commun.* **2021**, *12*, 5662.
- [7] Y. Zhuang, D. Chen, W. Chen, W. Zhang, X. Su, R. Deng, Z. An, H. Chen, R.-J. Xie, *Light Sci. Appl.* **2021**, *10*, 132.
- [8] R. Pu, Q. Zhan, X. Peng, S. Liu, X. Guo, L. Liang, X. Qin, Z. W. Zhao, X. Liu, *Nat. Commun.* **2022**, *13*, 6636.
- [9] N. Panov, D. Lu, E. Ortiz-Rivero, E. Martinazzo Rodrigues, P. Haro-González, D. Jaque, E. Hemmer, *Adv. Opt. Mater.* **2021**, *9*, 2100101.
- [10] Y.L. Li, N.N. Li, D. Wang, F. Chu, S.D. Lee, Y.W. Zheng, Q.H. Wang, *Light Sci. Appl.* **2022**, *11*, 188.
- [11] H. Zhou, X. Zeng, A. Li, W. Zhou, L. Tang, W. Hu, Q. Fan, X. Meng, H. Deng, L. Duan, Y. Li, Z. Deng, X. Hong, Y. Xiao, *Nat. Commun.* **2020**, *11*, 6183.
- [12] K. Zhanghao, X. Chen, W. Liu, M. Li, Y. Liu, Y. Wang, S. Luo, X. Wang, C. Shan, H. Xie, J. Gao, X. Chen, D. Jin, X. Li, Y. Zhang, Q. Dai, P. Xi, *Nat. Commun.* **2019**, *10*, 4694.
- [13] J. Kim, S. Michelin, M. Hilbers, L. Martinelli, E. Chaudan, G. Amselem, E. Fradet, J.-P. Boilot, A. M. Brouwer, C. N. Baroud, J. Peretti, T. Gacoin, *Nat. Nanotechnol.* **2017**, *12*, 914.
- [14] J. Kim, R. Chacón, Z. Wang, E. Larquet, K. Lahlil, A. Leray, G. Colas-des-Francis, J. Kim, T. Gacoin, *Nat. Commun.* **2021**, *12*, 1943.
- [15] K. Du, J. Feng, X. Gao, H. Zhang, *Light Sci. Appl.* **2022**, *11*, 222.
- [16] B. Yao, P. Lin, H. Sun, S. Wang, C. Luo, Z. Li, X. Du, Y. Ding, Y. Xu, H. Wan, W. Zhu, *Adv. Opt. Mater.* **2020**, *9*, 2001434.
- [17] X. Lai, Q. Ren, F. Vogelbacher, W. E. I. Sha, X. Hou, X. Yao, Y. Song, M. Li, *Adv. Mater.* **2021**, *34*, 2107243.
- [18] W. Yao, Q. Tian, W. Wu, *Adv. Opt. Mater.* **2018**, *7*, 1801171.
- [19] P. Li, F. Li, X. Zhang, Y. Li, X. Luo, R. Wang, Y. Cai, Y. Zhang, *Adv. Opt. Mater.* **2020**, *8*, 2000583.
- [20] Y. Xie, Y. Song, G. Sun, P. Hu, A. Bednarkiewicz, L. Sun, *Light Sci. Appl.* **2022**, *11*, 150.
- [21] X. Zhou, L. Ning, J. Qiao, Y. Zhao, P. Xiong, Z. Xia, *Nat. Commun.* **2022**, *13*, 7589.
- [22] X. Chen, Y. Liu, D. Tu, *Lanthanide-Doped Luminescent Nanomaterials*, Springer Berlin Heidelberg, Berlin, Heidelberg, **2014**.
- [23] D. Yang, Z. Peng, X. Guo, S. Qiao, P. Zhao, Q. Zhan, J. Qiu, Z. Yang, G. Dong, *Adv. Opt. Mater.* **2021**, *9*, 2100044.
- [24] D. Yang, Z. Peng, Q. Zhan, X. Huang, X. Peng, X. Guo, G. Dong, J. Qiu, *Small* **2019**, *15*, 1904298.
- [25] P. Chen, M. Song, E. Wu, B. Wu, J. Zhou, H. Zeng, X. Liu, J. Qiu, *Nanoscale* **2015**, *7*, 6462.
- [26] Z.-Y. Lyu, H. Dong, X.-F. Yang, L.-D. Sun, C.-H. Yan, *J. Phys. Chem. Lett.* **2021**, *12*, 11288.
- [27] L. Chen, Y. Rong, M. Ren, W. Wu, M. Qin, C. Pan, Q. Ma, S. Liu, B. Wu, E. Wu, J. Xu, H. Zeng, *J. Phys. Chem. C* **2018**, *122*, 15666.
- [28] J. He, W. Zheng, F. Ligmajer, C.-F. Chan, Z. Bao, K.-L. Wong, X. Chen, J. Hao, J. Dai, S.-F. Yu, D. Y. Lei, *Light Sci. Appl.* **2017**, *6*, e16217.
- [29] D. Tu, Y. Liu, H. Zhu, R. Li, L. Liu, X. Chen, *Angew. Chem.* **2012**, *125*, 1166.
- [30] J. B. Gruber, M. E. Hills, R. M. MacFarlane, C. A. Morrison, G. A. Turner, *Chem. Phys.* **1989**, *134*, 241.
- [31] R. Kolesov, K. Xia, R. Reuter, R. Stöhr, A. Zappe, J. Meijer, P. R. Hemmer, J. Wrachtrup, *Nat. Commun.* **2012**, *3*, 1029.

- [32] J. Zhou, G. Chen, Y. Zhu, L. Huo, W. Mao, D. Zou, X. Sun, E. Wu, H. Zeng, J. Zhang, L. Zhang, J. Qiu, S. Xu, *J. Mater. Chem. C* **2014**, *3*, 364.
- [33] X. Huang, S. Han, W. Huang, X. Liu, *Chem. Soc. Rev.* **2013**, *42*, 173.
- [34] M. Pollnau, D. R. Gamelin, S. R. Lüthi, H. U. Güdel, M. P. Hehlen, *Phys. Rev. B* **2000**, *61*, 3337.
- [35] H. Liu, K. Huang, R. R. Valiev, Q. Zhan, Y. Zhang, H. Ågren, *Laser Photonics Rev.* **2017**, *12*, 1700144.
- [36] J. F. Suyver, A. Aebischer, S. García-Revilla, P. Gerner, H. U. Güdel, *Phys. Rev. B* **2005**, *71*, 125123.
- [37] R. Martín-Rodríguez, A. Meijerink, *J. Lumin.* **2014**, *147*, 147.
- [38] P. Villanueva-Delgado, K. W. Krämer, R. Valiente, *J. Phys. Chem. C* **2015**, *119*, 23648.
- [39] F. Wang, Y. Han, C. S. Lim, Y. Lu, J. Wang, J. Xu, H. Chen, C. Zhang, M. Hong, X. Liu, *Nature* **2010**, *463*, 1061.
- [40] H. He, J. Liu, K. Li, Z. Yin, J. Wang, D. Luo, Y. J. Liu, *Nano Lett.* **2020**, *20*, 4204.



TOC



## Supplementary Information

### Regulated Polarization Degree of Upconversion Luminescence and Multiple Anti-Counterfeit Applications

*Dongping Wen <sup>a</sup>, Yi Liang <sup>a</sup>, Xiaoming Mo <sup>a</sup>, Caofeng Pan <sup>a,b,\*</sup> and Ping Chen <sup>a\*</sup>*

<sup>a</sup> Center on Nanoenergy Research, Guangxi Key Laboratory for Relativistic Astrophysics, School of Physical Science and Technology, Guangxi University, Nanning 530004, P. R. China

<sup>b</sup> CAS Center for Excellence in Nanoscience, Beijing Key Laboratory of Micronano Energy and Sensor, Beijing Institute of Nanoenergy and Nanosystems, Chinese Academy of Sciences, Beijing, 100140, P. R. China

\*Corresponding authors

Prof. Ping Chen

Email: chenping@gxu.edu.cn

Prof. Caofeng Pan

Email: cfpan@binn.cas.cn

## Supplementary Section 1: Single-Particle Nanorod Microscopic Testing System

Upconversion luminescence was collected by a home-built optical microscope system, as shown in **Figure 2a**. A 1150 nm or 980 nm laser was focused on a sample located at the surface of a microscope slide by a microscope objective with a high numerical aperture (NA) (i.e., 100X, NA = 1.3).

The numerical aperture was defined as:

$$NA = n * \sin \theta, \quad (1)$$

where  $n$  is the refractive index of the medium between lens and sample,  $\theta$  is the half degree of divergence of the beam.

The spot size was calculated by

$$d = (1.22 * \lambda) / NA, \quad (2)$$

where  $\lambda$  is the excitation wavelength, and  $d$  is the spot size. Thus, the spot size of the 1150 nm excitation beam was estimated to be about 1080 nm in diameter.

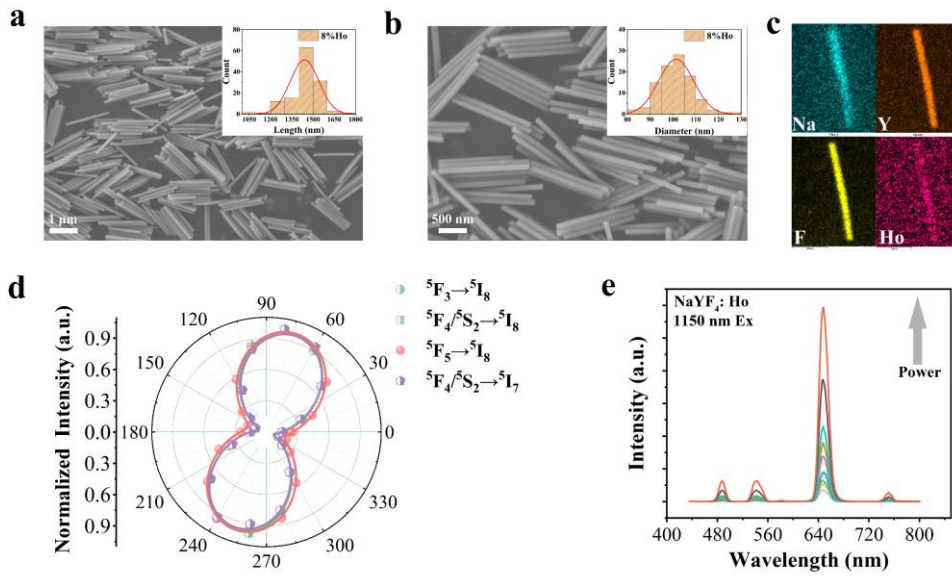


**Figure S1. SEM images and spectroscopic testing of NaYF<sub>4</sub>:Ho nanorods.** (a-b) SEM images of NaYF<sub>4</sub>: 8% Ho nanorod; the insets are histogram showing the size in (a) *c* and (b) *a* axis. (c) Energy dispersive spectrum (EDS) mapping of NaYF<sub>4</sub>:Ho single nanorod. (d) Polar plots the upconversion luminescence integral intensities from  $^5F_3 \rightarrow ^5I_8$ ,  $^5F_4/^5S_2 \rightarrow ^5I_8$ ,  $^5F_5 \rightarrow ^5I_8$  transitions as a function of the excitation polarization angle. (e) UCL spectra with different excitation powers.

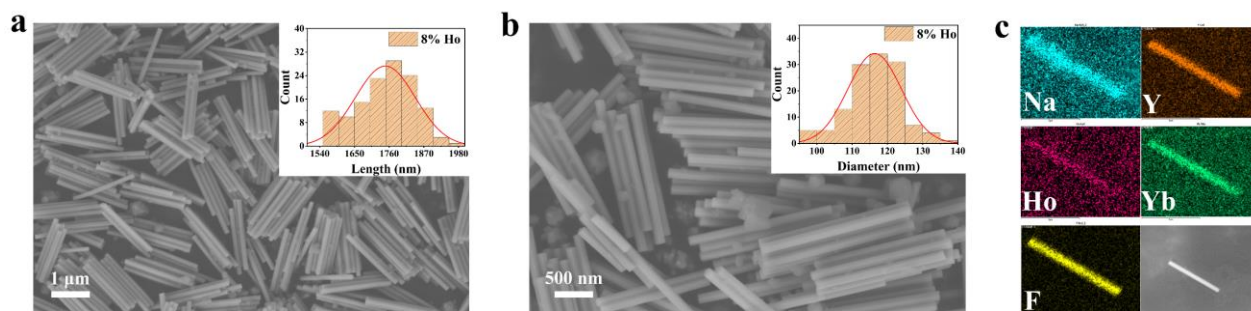


**Figure S2. SEM images and EDS mapping.** (a-b) SEM images of NaYF<sub>4</sub>: 8% Ho, 20% Yb nanorod. Insets are size histograms on the (a) *c* and (b) *a* axes. (c) EDS mapping of NaYF<sub>4</sub>: 8% Ho, 20% Yb single nanorod.

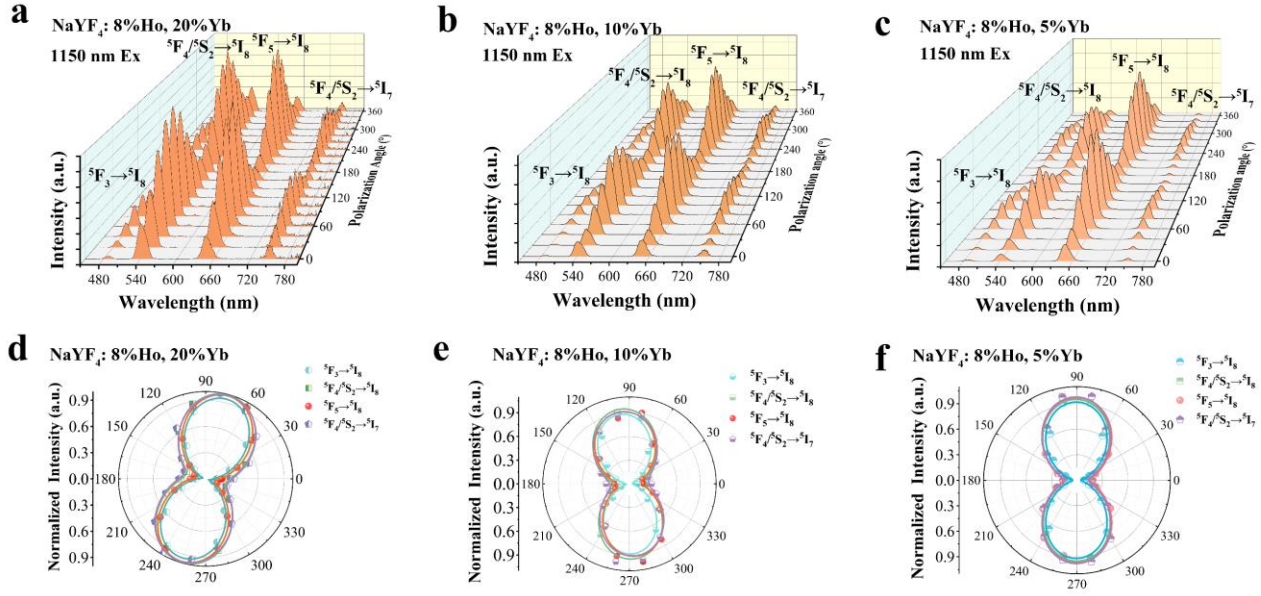


**Figure S3. Spectroscopic testing of NaYF<sub>4</sub>:Yb,Ho single nanoroad by 1150 nm laser.** (a-c) PUCL spectra from NaYF<sub>4</sub>: x% Yb, 8% Ho (x = 20 (a), 10 (b), 5 (c)) single nanoroad. (d-f) Polar plots upconversion luminescence integral intensities as a function of the excitation polarization angle from NaYF<sub>4</sub>: 8% Ho, x% Yb (x = 20 (d), 10 (e), 5 (f)) single nanorods.



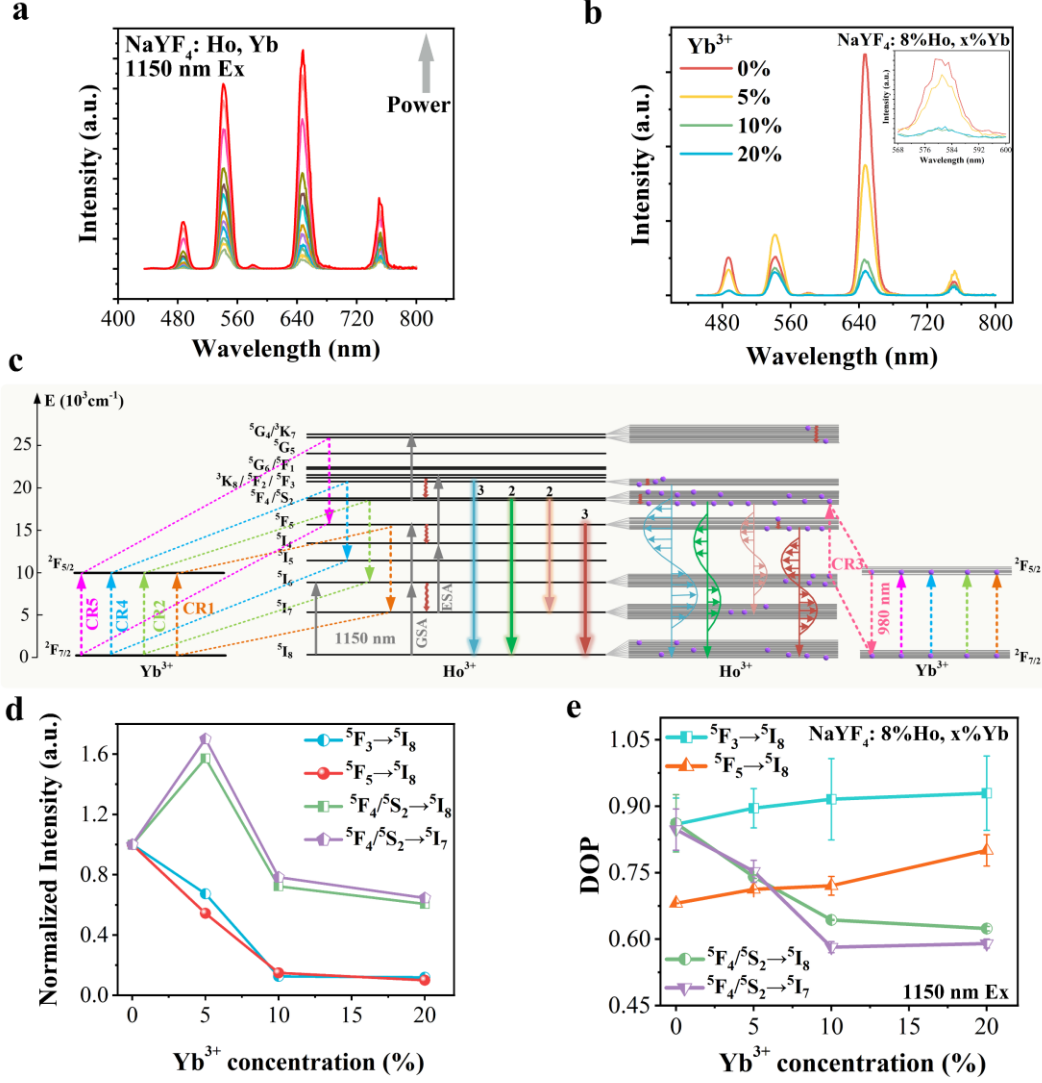


**Figure S4. Cross-relaxation in NaYF<sub>4</sub>:Ho,Yb nanorods by 1150 nm laser.** (a) UCL spectra with different excitation powers from NaYF<sub>4</sub>: 8% Ho, 20% Yb nanorods. (b) UCL spectra with various concentrations of Yb<sup>3+</sup>. Inset is the UCL spectra of <sup>5</sup>G<sub>4</sub>/<sup>5</sup>K<sub>7</sub> → <sup>5</sup>I<sub>7</sub>. (c) Schematic illustration of the multiphoton upconversion of NaYF<sub>4</sub>:Yb,Ho excited at 1150 nm with DOPs of PUCL from different ESs. (d) Dependence normalized integrated intensity of UCL on Yb<sup>3+</sup> concentration. (e) Dependence of DOPs for four transitions on the concentration of Yb<sup>3+</sup>.

The cross-relaxation (CR) of Ho<sup>3+</sup> and Yb<sup>3+</sup> causes the abnormal photon number in NaYF<sub>4</sub>: Yb, Ho. When introducing Yb<sup>3+</sup> into Ho<sup>3+</sup>-doped NaYF<sub>4</sub> nanorods, five kinds of CR between Yb<sup>3+</sup> and Ho<sup>3+</sup> occur (Figure S4c).

CR1 is <sup>5</sup>F<sub>5</sub>(Ho<sup>3+</sup>) + <sup>2</sup>F<sub>7/2</sub>(Yb<sup>3+</sup>) → <sup>5</sup>I<sub>7</sub>(Ho<sup>3+</sup>) + <sup>2</sup>F<sub>5/2</sub>(Yb<sup>3+</sup>). Once introducing Yb<sup>3+</sup> into nanorods, the luminescence intensity from <sup>5</sup>F<sub>5</sub> → <sup>5</sup>I<sub>8</sub> is largely reduced (Figure S4b and S4d). And the luminescence intensity decreases gradually with increasing Yb<sup>3+</sup> concentration, indicating the CR1 between Yb<sup>3+</sup> and Ho<sup>3+</sup> [1].

CR3 is <sup>5</sup>I<sub>6</sub>(Ho<sup>3+</sup>) + <sup>2</sup>F<sub>5/2</sub>(Yb<sup>3+</sup>) → <sup>5</sup>F<sub>4</sub>/<sup>5</sup>S<sub>2</sub>(Ho<sup>3+</sup>) + <sup>2</sup>F<sub>7/2</sub>(Yb<sup>3+</sup>). With increasing Yb<sup>3+</sup> concentration from 0% to 5%, luminescence intensities from <sup>5</sup>F<sub>4</sub>/<sup>5</sup>S<sub>2</sub> → <sup>5</sup>I<sub>8</sub> and <sup>5</sup>F<sub>4</sub>/<sup>5</sup>S<sub>2</sub> → <sup>5</sup>I<sub>7</sub> transitions are enhanced (Figure S4b and S4d), suggesting CR3 between Yb<sup>3+</sup> and Ho<sup>3+</sup> [1].

CR2 is <sup>5</sup>F<sub>4</sub>/<sup>5</sup>S<sub>2</sub>(Ho<sup>3+</sup>) + <sup>2</sup>F<sub>7/2</sub>(Yb<sup>3+</sup>) → <sup>5</sup>I<sub>6</sub>(Ho<sup>3+</sup>) + <sup>2</sup>F<sub>5/2</sub>(Yb<sup>3+</sup>). When increasing Yb<sup>3+</sup> concentration from 5% to 20%, luminescence intensities from <sup>5</sup>F<sub>4</sub>/<sup>5</sup>S<sub>2</sub> → <sup>5</sup>I<sub>8</sub> and <sup>5</sup>F<sub>4</sub>/<sup>5</sup>S<sub>2</sub> → <sup>5</sup>I<sub>7</sub> transitions are decreased (Figure S4b and S4d), suggesting CR2 between Yb<sup>3+</sup> and Ho<sup>3+</sup> [1].

CR4 is  $^5F_3(\text{Ho}^{3+}) + ^2F_{7/2}(\text{Yb}^{3+}) \rightarrow ^5I_5(\text{Ho}^{3+}) + ^2F_{5/2}(\text{Yb}^{3+})$ . Once introducing  $\text{Yb}^{3+}$  into nanorods, the luminescence intensity of  $^5F_3 \rightarrow ^5I_8$  is largely reduced (Figure S4b and S4d). And the luminescence intensity decreases gradually with increasing  $\text{Yb}^{3+}$  concentration, indicating the CR4 between  $\text{Yb}^{3+}$  and  $\text{Ho}^{3+}$  [1].

CR5 is  $^5G_4/^3K_7(\text{Ho}^{3+}) + ^2F_{7/2}(\text{Yb}^{3+}) \rightarrow ^5F_5(\text{Ho}^{3+}) + ^2F_{5/2}(\text{Yb}^{3+})$ . When increasing  $\text{Yb}^{3+}$  concentration, luminescence intensities from the  $^5G_4/^3K_7 \rightarrow ^5I_7$  transition are decreased and even disappear at 20% and 10%  $\text{Yb}^{3+}$  concentration (Figure S4b and S4d), suggesting CR5 between  $\text{Yb}^{3+}$  and  $\text{Ho}^{3+}$  [1].

$^5F_4/^5S_2 \rightarrow ^5I_8$  and  $^5F_4/^5S_2 \rightarrow ^5I_7$  transitions are changed from three-photon process in  $\text{NaYF}_4:\text{Ho}$  single nanorod to two-photon process in  $\text{NaYF}_4:\text{Yb},\text{Ho}$  single nanorod, resulting in reduced DOPs in  $\text{NaYF}_4:\text{Yb},\text{Ho}$  single nanorod (Figure S4e). For the same transition from  $^5F_4/^5S_2$  states, three-photon upconversion pumps a lower population density and gives a higher DOP of PUCL compared with the two-photon process. Those results show that the DOPs of PUCL are mainly determined by population density in ESs and not the energy levels themselves.

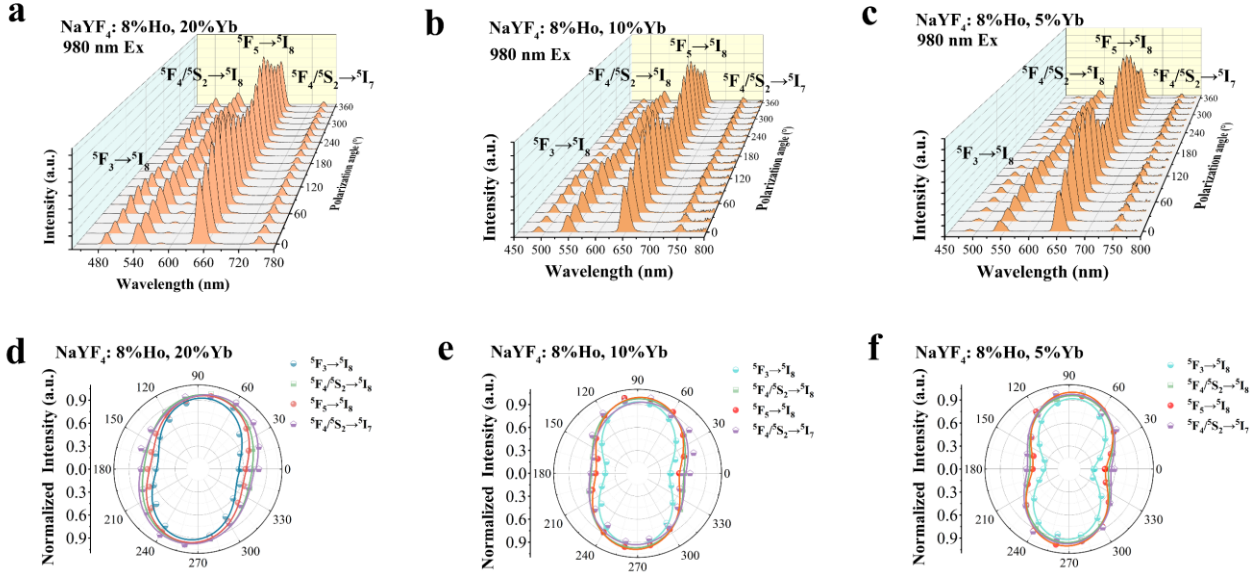


**Figure S5. PUCL spectra of NaYF<sub>4</sub>:Ho,Yb nanorods excited by 980 nm laser.** (a-c) PUCL spectra from NaYF<sub>4</sub>: 8% Ho, y% Yb (y = 20 (a), 10 (b), 5(c)) single nanorods. (d-f) Polar plots upconversion luminescence integral intensities as a function of the excitation polarization angle from NaYF<sub>4</sub>: 8% Ho, y% Yb (y = 20 (d), 10 (e), 5 (f)) single nanorods.

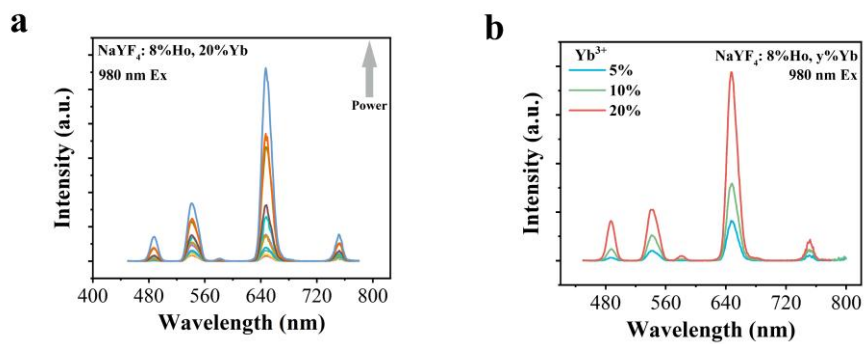


**Figure S6. Upconversion luminescence spectra of NaYF<sub>4</sub>:Ho,Yb nanorods excited by 980 nm.** (a) Upconversion luminescence spectra from a NaYF<sub>4</sub>: 8% Ho, 20% Yb single nanorod with different excitation powers. (b) Upconversion luminescence spectra from NaYF<sub>4</sub>: 8% Ho, y% Yb (y = 5, 10, 20) single nanorods under the same excitation power.

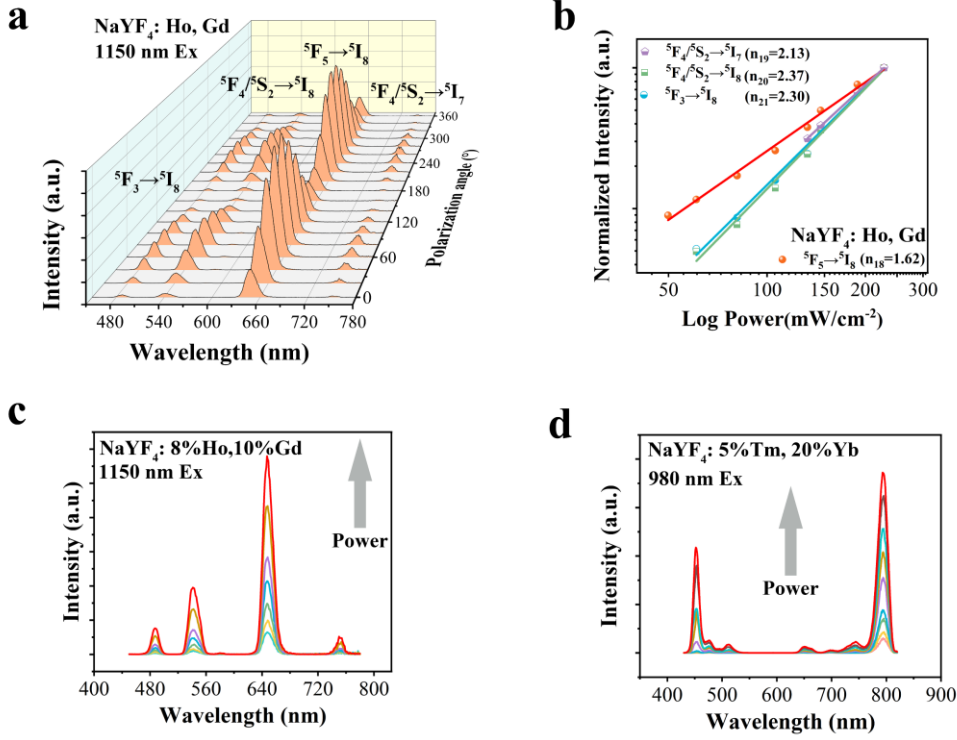


**Figure S7. PUCL spectra of NaYF<sub>4</sub>:Ho,Gd nanoroads excited by 1150 nm.** (a) PUCL spectra of NaYF<sub>4</sub>: 8% Ho, 10% Gd single nanorod with exciting polarization angles of 1150 nm from 0° to 360°. (b) Normalized intensities of NaYF<sub>4</sub>: 8% Ho, 10% Gd single nanorod as a function of excitation power at 1150 nm. (c-d) Upconversion luminescence spectra of NaYF<sub>4</sub>: 8% Ho, 10% Gd (c) and NaYF<sub>4</sub>: 5% Tm, 20% Yb (d) single nanorods with different excitation powers.

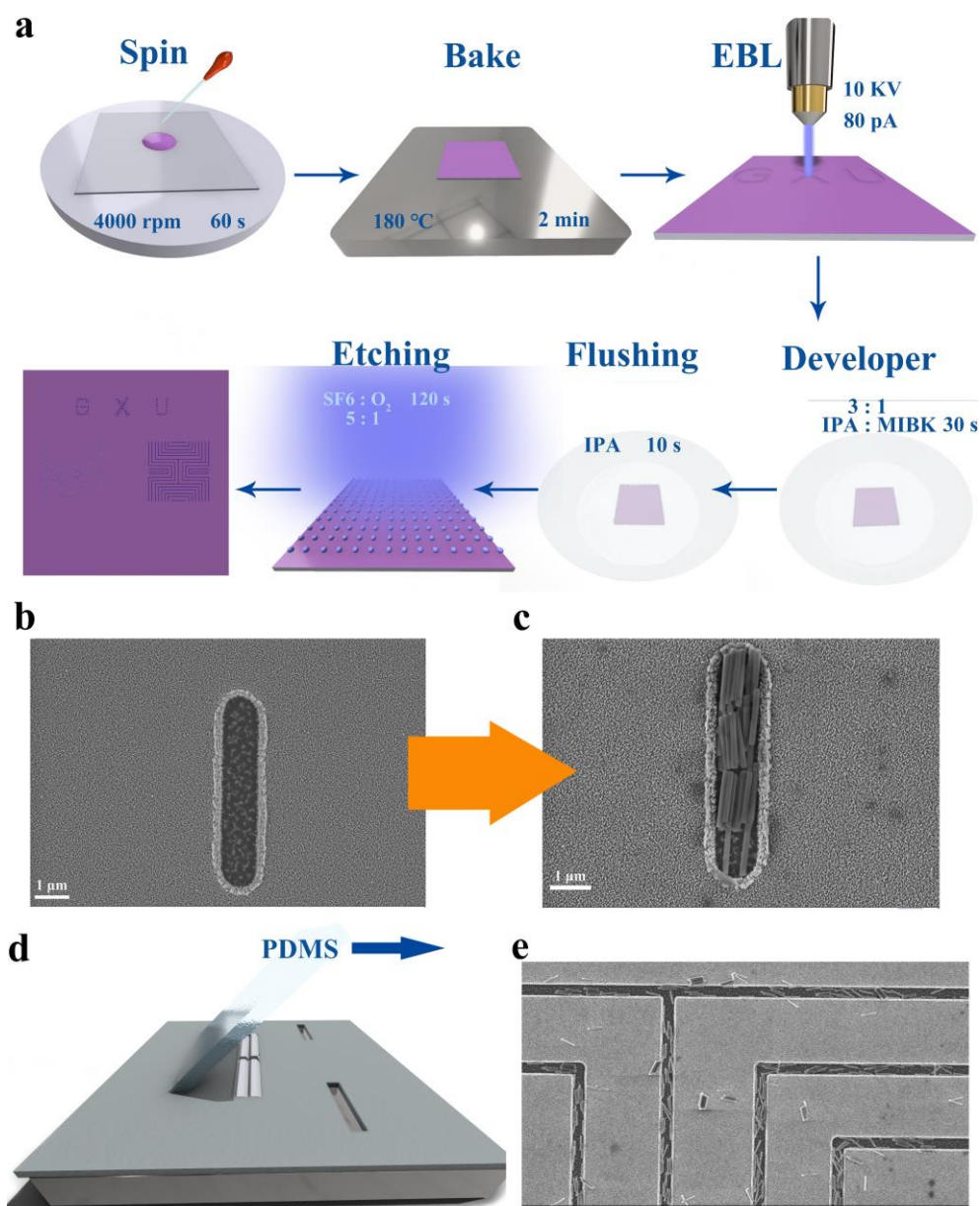


**Figure S8. SEM images of the rectangular groove and nanowire groove as pixel points.** (a) Schematic diagram of the template manufacturing process. (b) SEM image of a rectangular groove with etching by EBL and RIE. (c) SEM image of rectangular groove filled by NaYF<sub>4</sub>:Yb,Ho nanorods. (d) Demonstration of the method of assembling nanorods by PDMS. (e) SEM image of nanowire groove are filled by NaYF<sub>4</sub>:Yb,Ho nanorods.



## References

- [1] R. Martín-Rodríguez, A. Meijerink, *J. Lumin.* **2014**, *147*, 147.